Table 8. *Mean inner potentials in* V *calculated using Doyle–Turner electron scattering factors, the Herman–Skillman Hartree–Slater program and the Grant et al.* (1980) *Dirac–Fock program*

| | Doyle–Turner | Herman–Skillman | Dirac–Fock |
|---|---|---|---|
| Aluminium | 17.10 | 15.59 | 17.04 |
| Silicon | 14.02 | 13.42 | 13.84 |
| Copper | 22.06 | 21.51 | 24.35 |
| Germanium | 15.58 | 14.64 | 15.57 |
| Silver | 24.44 | 23.24 | 24.36 |
| Gold | 29.80 | 27.90 | 29.73 |
| $SiO_2$ neutral | 6.87 | 10.16 | 6.89 |
| MgO neutral | 18.34 | 17.45 | 18.40 |
| MgO ions | | 11.48 | 12.64 |
| GaAs | 15.19 | 14.41 | 15.40 |

applied to other systems, such as intermetallics, and how the results would compare with measurements from energy-loss fine structure.

## Concluding remarks

We have presented X-ray scattering-factor tables for a complete range of elements and ions calculated using a multiconfiguration Dirac–Fock computer code. The results are within less than 1% of the relativistic Hartree–Fock results of Doyle & Turner (1968). We have also given two parameterizations in terms of four Gaussians, one of higher accuracy over a range of about 2.0 $Å^{-1}$ and the other of lower accuracy over an extended range of 6.0 $Å^{-1}$. In general, we recommend direct use of the tables rather than use of the parameterizations. The electron scattering factors can be calculated from the X-ray scattering factors using the Mott formula. The limiting case of $f_{el}(0)$ has been tabulated directly and can be used to calculate the mean inner potential. We show that the mean inner potential can be very sensitive to charge transfer and we give estimates for a number of compounds for which measurements are available.

Information on how to obtain the complete tables is available from DR at the address given above.

The multiconfiguration Dirac–Fock calculations that form the basis of this paper were performed on a VAX system at the Cavendish Laboratory, Cambridge. We acknowledge Professors A. Howie and L. M. Brown for providing access to these facilities and Dr A. Bleloch for his help. We also acknowledge useful discussions with Drs J. M. Zuo, J. C. H. Spence, M. A. O'Keefe and A. G. Fox.

### References

COWAN, R. D. (1981). *The Theory of Atomic Structure and Spectra*. Berkeley: Univ. of California Press.
CROMER, D. T. & WABER, J. T. (1965). *Acta Cryst.* **18**, 105–109.
DOYLE, P. A. & TURNER, P. S. (1968). *Acta Cryst.* A**24**, 390–397.
FOX, A. G., O'KEEFE, M. A. & TABBERNOR, M. A. (1989). *Acta Cryst.* A**45**, 786–793.
GAJDARDZISKA-JOSIFOVSKA, M., MCCARTNEY, M. R., DE RUIJTER, W. J., SMITH, D. J., WEISS, J. K. & ZUO, J. M. (1993). *Ultramicroscopy*, **50**, 285–299.
GRANT, I. P., MCKENZIE, B. J., NORRINGTON, P. H., MAYERS, D. F. & PYPER, N. C. (1980). *Comput. Phys. Commun.* **21**, 207–231.
HERMAN, F. & SKILLMAN, S. (1963). *Atomic Structure Calculations*. Englewood Cliffs, NJ: Prentice Hall.
IBERS, J. A. (1958). *Acta Cryst.* **11**, p. 178.
LIBERMAN, D. A., CROMER, D. T. & WABER, J. T. (1971). *Comput. Phys. Commun.* **2**, 107–113.
MASLEN, E. N., FOX, A. G. & O'KEEFE, M. A. (1992). *International Tables for Crystallography*, Vol. C, edited by A. J. C. WILSON, Section 6.1.1, pp. 476–511. Dordrecht: Kluwer Academic Publishers.
O'KEEFFE, M. & SPENCE, J. C. H. (1994). *Acta Cryst.* A**50**, 33–45.
PRESS, W. H., FLANNERY, B. P., TEUKOLSKY, J. A. & VETTERLING, W. T. (1989). *Numerical Recipes*. Cambridge Univ. Press.
ROSS, F. M. & STOBBS, W. M. (1991). *Philos. Mag.* A**63**, 1–36.
SHIH, W. C. & STOBBS, W. M. (1990). *Ultramicroscopy*, **32**, 219–239.
WATSON, R. E. (1958). *Phys. Rev.* **111**, 1108–1110.
WEICKENMEIER, A. & KOHL, H. (1991). *Acta Cryst.* A**47**, 590–597.

*Acta Cryst.* (1994). A**50**, 497–503

# Use of Tilted Bragg Reflections in X-ray Standing-Wave Experiments and X-ray Optics Applications

BY A. TACCOEN, C. MALGRANGE, Y. L. ZHENG, J. C. BOULLIARD AND B. CAPELLE

*Laboratoire de Minéralogie et Cristallographie, Universités Paris* 6 *et* 7, *CNRS URA* 09, 4 *place Jussieu*, 75252 *Paris CEDEX* 05, *France*

(*Received* 5 *November* 1993; *accepted* 11 *March* 1994)

## Abstract

This paper studies in detail 'tilted reflections', which are defined here as Bragg reflections where the incident vector $\mathbf{k}_o^{(a)}$, the diffraction vector $\mathbf{h}$ and the normal $\mathbf{n}$ to the surface are not coplanar. Such reflections are especially useful when it is necessary to work in Bragg geometry with reflecting planes

making an angle $\Phi$ with the crystal surface that is larger than the Bragg angle. It is shown that the usual expressions of X-ray dynamical theory can still be applied if the vector **n** normal to the crystal surface is replaced by its projection **n**′ on the diffraction plane $(\mathbf{h},\mathbf{k}_o^{(a)})$ (except naturally when **n**′ is a null or nearly null vector). By rotation of the crystal surface around the diffraction vector, one can then go from transmission cases to reflection ones with various asymmetry factors. Tilted reflections are used in X-ray standing-wave experiments to triangulate atomic positions. It is shown and illustrated by experimental results that an accurate determination of the asymmetry factor is then necessary for correct analysis of the results.

## 1. Introduction

Since its first development by Batterman (1964, 1969), the X-ray standing-wave (XSW*) method has been used for the study of surfaces and interfaces. Much work on the determination of the positions of adsorbed atoms on the surface of semiconductors such as silicon (Bedzyk, Gibson & Golovchenko, 1982; Vlieg, Fontes & Patel, 1991; Boulliard *et al.*, 1992), gallium arsenide (Saitoh, Hashizume & Tsutsui, 1988) and germanium (Bedzyk & Materlick, 1985) has been reported. An XSW experiment allows one to determine the relative positions of adatoms (adsorbed atoms) with respect to the reflecting planes by simultaneously recording the rocking curve of the substrate for the selected reflection and the fluorescence yield of the adatoms. Use of different reflections allows determination of the positions by triangulation. The crystal surface generally has low $h$, $k$, $l$ indices and a symmetric reflection on the $(hkl)$ planes determines the positions of adatoms perpendicular to the surface. Then, reflections using two other reflecting planes inclined by angles $\Phi_1$ and $\Phi_2$ with respect to the surface are used to fully determine the positions of the atoms with respect to the crystal. This $\Phi_i$ angle $(i = 1, 2)$, between the normal to the crystal surface **n** oriented inwards and the diffraction vector **h**, can be larger than the Bragg angle $\theta_B$; then, usual asymmetric reflection where the incident wave vector $\mathbf{k}_o^{(a)}$, the diffraction vector **h** and the normal **n** are coplanar would lead to a Laue transmission geometry. In order to have Bragg reflection geometry, it is necessary to turn the crystal around the diffraction vector **h** (Fig. 1). The plane **(h,n)** and the diffraction plane $(\mathbf{h},\mathbf{k}_o^{(a)})$ then make an angle $\beta$. Such reflections with $\beta \neq 0$ are hereinafter referred to as tilted reflections. $\beta = 0$ (and $\Phi \neq 0$) corresponds to the usual asymmetric Laue geometry.

The aim of this paper is to point out the exact geometrical parameters that have to be taken into account in tilted geometries in order to correctly calculate the theoretical rocking curves and fluorescence yields in XSW experiments and to underline the importance of the adjustment of the $\beta$ angle. Rocking curves for a $11\bar{1}$ reflection ($\Phi = 70.52°$) of an Si(111) crystal have been measured as a function of $\beta$. For the same reflection, XSW experiments with different $\beta$ angles have been performed on an Si(111) crystal with three iron monolayers (MLs) deposited ($1\ \text{ML} = 0.78 \times 10^{15}$ atoms $\text{cm}^{-2}$). The results emphasize the importance of very precise knowledge of this angle $\beta$ for the reliability of the XSW results.

## 2. Fundamental equations for an XSW experiment, rocking curve and fluorescence yield

In the following paragraphs, Authier's (1986) notation for the X-ray dynamical theory is used; in this formulation, the vector **n** is oriented into the crystal.

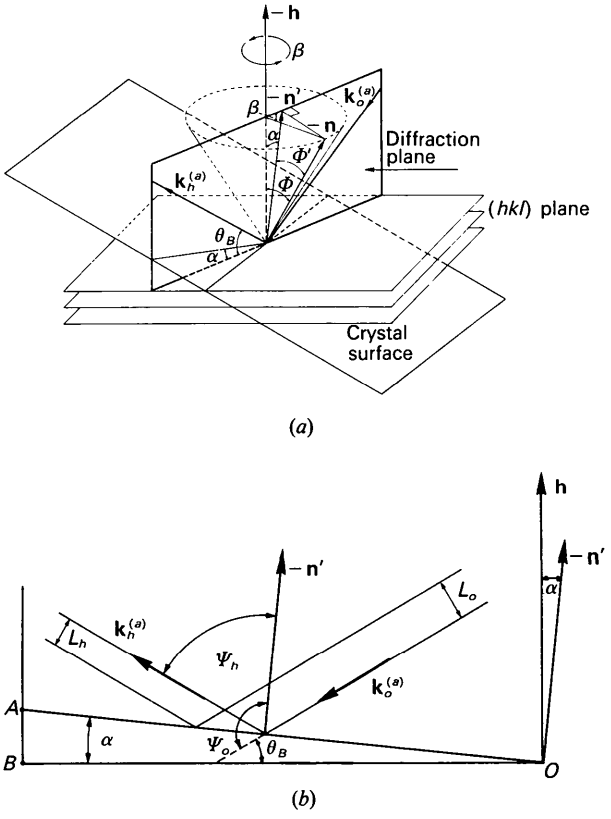


Fig. 1. Geometrical description of a tilted reflection: (*a*) general view; (*b*) figure in the diffraction plane $(\mathbf{h},\mathbf{k}_o^{(a)})$.

* The case of XSW at normal incidence is not taken into account here.

2.1. *Standing waves*

Bragg diffraction of a plane wave in a perfect thick crystal induces an electric field **D** equal to

$$\mathbf{D}(\mathbf{r},\theta) = \mathbf{D}_o(\theta)\exp(-i2\pi\mathbf{k}_o\cdot\mathbf{r}) + \mathbf{D}_h(\theta)\exp(-i2\pi\mathbf{k}_h\cdot\mathbf{r}), \quad (1)$$

where $\theta$ is the angle of incidence with the diffracting planes, $D_o$ and $D_h$ are the amplitudes of the incident and diffracted waves inside the crystal, $\mathbf{k}_o$ and $\mathbf{k}_h$ are their wave vectors and $\mathbf{h}$ is the reciprocal-lattice vector associated with the *hkl* reflection. These three vectors are linked together by $\mathbf{k}_h = \mathbf{k}_o - \mathbf{h}$.

The interference between the two waves creates a standing wave whose intensity is

$$|\mathbf{D}(\mathbf{r},\theta)|^2 = |\mathbf{D}_o(\theta)|^2\{1 + |\xi(\theta)|^2 + 2C|\xi(\theta)|\cos[\psi(\theta) + 2\pi\mathbf{h}\cdot\mathbf{r}]\}, \quad (2)$$

where $C = 1$ or $\cos 2\theta$ according to the direction of the electric vector either normal or parallel to the diffraction plane $(\mathbf{h},\mathbf{k}_o^{(a)})$ and $\xi(\theta)$ is the ratio of the complex amplitudes $D_h(\theta)$ and $D_o(\theta)$ whose phase is $\psi(\theta)$:

$$\xi(\theta) = D_h(\theta)/D_o(\theta) = [|\mathbf{D}_h(\theta)|/|\mathbf{D}_o(\theta)|]\exp[i\psi(\theta)]. \quad (3)$$

2.2. *Rocking curve*

The measured reflecting power $I_h$ is the ratio of the diffracted and the incident energies outside the crystal and is given by

$$I_h(\theta) = |\gamma|[|\mathbf{D}_h^{(a)}(\theta)|^2/|\mathbf{D}_o^{(a)}|^2], \quad (4)$$

where $\mathbf{D}_o^{(a)}$ and $\mathbf{D}_h^{(a)}$ are the incident and diffracted waves outside the crystal and $|\gamma|$ is the ratio of the cross sections of the corresponding beams.

Boundary conditions simply link $\mathbf{D}_o^{(a)}$ and $\mathbf{D}_h^{(a)}$ to $\mathbf{D}_o$ and $\mathbf{D}_h$ waves inside the crystal by $\mathbf{D}_o^{(a)} = \mathbf{D}_o$, $\mathbf{D}_h^{(a)} = \mathbf{D}_h$ and

$$I_h(\theta) = |\gamma|[|\mathbf{D}_h(\theta)|^2/|\mathbf{D}_o(\theta)|^2] = |\gamma||\xi(\theta)|^2. \quad (5)$$

The ratio $|\gamma|$ of the cross sections $L_h$ and $L_o$ (Fig. 1*b*) of the diffracted and incident beams plays the role of the usual asymmetry factor:

$$\gamma = \gamma_h/\gamma_o = \cos\Psi_h/\cos\Psi_o, \quad (6)$$

where $\Psi_o = (\mathbf{n}',\mathbf{k}_o^{(a)})$ and $\Psi_h = (\mathbf{n}',\mathbf{k}_h^{(a)})$, $\mathbf{n}'$ being the projection of $\mathbf{n}$ on the $(\mathbf{h},\mathbf{k}_o^{(a)})$ plane (Fig. 1*b*). Let us call the angle $\alpha$, $\alpha = (\mathbf{n}',\mathbf{h})$, the asymmetry angle. Then, $\Psi_o = \pi/2 + \theta_B + \alpha$, $\Psi_h = \pi/2 - (\theta_B - \alpha)$ and $\gamma = -\sin(\theta_B - \alpha)/\sin(\theta_B + \alpha)$.

2.3. *Fluorescence yield*

Let us call $\rho(\mathbf{r})$ the atomic distribution of the adatoms whose fluorescence yield $Y(\theta)$ is recorded. Under the dipolar approximation (Zegenhagen, 1993), $Y(\theta)$ depends on the intensity of the electric field $|\mathbf{D}(\mathbf{r},\theta)|^2$ and the atomic distribution $\rho(\mathbf{r})$ through the relation

$$Y(\theta) \propto \int\rho(\mathbf{r})|\mathbf{D}(\mathbf{r},\theta)|^2\,\mathrm{d}^3r/\int\rho(\mathbf{r})\,\mathrm{d}^3r,$$

which becomes, from (2),

$$Y(\theta) \propto 1 + |\xi(\theta)|^2 + 2C|\xi(\theta)| \times\{\int\rho(\mathbf{r})\cos[\psi(\theta) + 2\pi\mathbf{h}\cdot\mathbf{r}]\mathrm{d}^3r/\int\rho(\mathbf{r})\,\mathrm{d}^3r\}. \quad (7)$$

This expression leads to the definition of the coherent fraction $F_h$ and the coherent position $P_h$ of the $\rho(\mathbf{r})$ distribution for the *hkl* reflection as the Fourier component of $\rho(\mathbf{r})$ with respect to the diffraction vector $\mathbf{h}$,

$$F_h\exp(i2\pi P_h) = \int\rho(\mathbf{r})\exp(i2\pi\mathbf{h}\cdot\mathbf{r})\,\mathrm{d}^3r/\int\rho(\mathbf{r})\,\mathrm{d}^3r. \quad (8)$$

Then, the fluorescence yield can be expressed as a function of $F_h$ and $P_h$ by

$$Y(\theta) \propto 1 + |\xi(\theta)|^2 + 2C|\xi(\theta)|F_h\cos[\psi(\theta) + 2\pi P_h]. \quad (9)$$

The interpretation of an XSW experiment relies on the precise determination of $F_h$ and $P_h$, which are obtained by a numerical two-step fit: (i) simulation of the experimental rocking curve to determine the experimental resolution function that convolutes the theoretical profiles; and (ii) simulation of the experimental fluorescence, using the resolution function determined in (i), to obtain the two parameters $F_h$ and $P_h$.

## 3. Calculation of $\xi(\theta)$

The propagation equation in the crystal gives for $\xi(\theta)$

$$\xi = D_h/D_o = 2X_o/kC\chi_{\bar{h}} = kC\chi_h/2X_h, \quad (10)$$

where $\chi_h$ and $\chi_{\bar{h}}$ are the $h$th and $\bar{h}$th Fourier components of the dielectric susceptibility and $k = |\mathbf{k}_o^{(a)}| = |\mathbf{k}_h^{(a)}|$. The quantities $X_o$ and $X_h$ are defined by

$$X_o = [\mathbf{k}_o^2 - k^2(1 + \chi_o)]/2k$$
$$X_h = [\mathbf{k}_h^2 - k^2(1 + \chi_o)]/2k. \quad (11)$$

$X_o$ and $X_h$ are related by the well known equation

$$X_oX_h = k^2C^2\chi_h\chi_{\bar{h}}/4, \quad (12)$$

The value of $\xi(\theta)$ is determined from the continuity condition of the tangential components of the wave vectors.

The usual construction in reciprocal space introduces the intersection $L_a$ of the two spheres of radii $k = 1/\lambda$ centred at the reciprocal-lattice points $O$ and $H$ with the $(\mathbf{h},\mathbf{k}_o^{(a)})$ plane (Fig. 2) and the common extremity of the wave vectors $\mathbf{k}_o$ and $\mathbf{k}_h$ called the

*tie-point P*:

$$\mathbf{k}_o = \mathbf{OP} \quad \text{and} \quad \mathbf{k}_h = \mathbf{HP}. \tag{13}$$

Outside the crystal, $\mathbf{k}_o^{(a)} = \mathbf{OM}$ is the incident wave vector. Thanks to (13), one gets $\mathbf{k}_o^{(a)} - \mathbf{k}_o = \mathbf{MP}$. Owing to the boundary conditions at the crystal surface, **MP** and **n** are collinear. For a tilted reflection, **h**, $\mathbf{k}_o^{(a)}$ and **n** are not coplanar and $\mathbf{k}_o$ is no longer in the $(\mathbf{h},\mathbf{k}_o^{(a)})$ plane, in contrast with the usual case of untilted reflections.

One can now obtain a second relation between $X_o$ and $X_h$ [(11)] by raising to the second power the equations

$$\begin{aligned} \mathbf{k}_o &= \mathbf{OP} = \mathbf{OL}_a + \mathbf{L}_a\mathbf{M} + \mathbf{MP} \\ \mathbf{k}_h &= \mathbf{HP} = \mathbf{HL}_a + \mathbf{L}_a\mathbf{M} + \mathbf{MP}. \end{aligned} \tag{14}$$

With only first-order terms kept:*

$$\begin{aligned} k_o^2 &= k^2 + 2\mathbf{OL}_a \cdot \mathbf{MP}, \\ k_h^2 &= k^2 + 2\mathbf{HL}_a \cdot \mathbf{L}_a\mathbf{M} + 2\mathbf{HL}_a \cdot \mathbf{MP}. \end{aligned} \tag{15}$$

The product $\mathbf{HL}_a \cdot \mathbf{L}_a\mathbf{M}$ is expressed by setting $L_aM = k\Delta\theta$, where $\Delta\theta$ is the departure from the Bragg angle. For tilted reflections, **MP** is not in the plane of diffraction. It is easy to check that $\mathbf{OL}_a \cdot \mathbf{MP} = \gamma_o\gamma_{\Phi'}k\overline{MP}$ and $\mathbf{HL}_a \cdot \mathbf{MP} = \gamma_h\gamma_{\Phi'}k\overline{MP}$, where $\gamma_{\Phi'} = \cos(\mathbf{n},\mathbf{n}')$ (Fig. 1). Equation (15) can be rewritten as

$$\begin{aligned} k_o^2 &= k^2 + 2k\overline{MP}\gamma_o\gamma_{\Phi'} \\ k_h^2 &= k^2 - 2k^2\Delta\theta \sin 2\theta + 2k\overline{MP}\gamma_h\gamma_{\Phi'}, \end{aligned} \tag{16}$$

* This development is valid for $\Phi$ angles smaller than 89.5°.

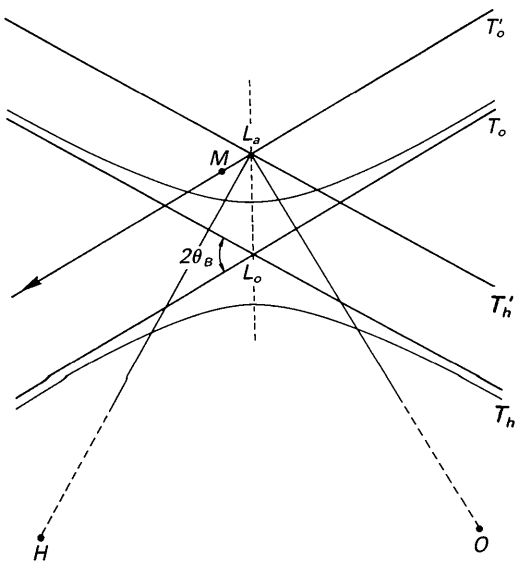


Fig. 2. Schematic drawing in the $(\mathbf{h},\mathbf{k}_o^{(a)})$ plane; $\mathbf{OM} = \mathbf{k}_o^{(a)}$. The normal **n** to the entrance surface issued from $M$ cuts the dispersion surface generated by a rotation of the hyperbola around **OH** at a point $P$ that is not located in the plane of the figure.

which gives for $X_o$ and $X_h$

$$\begin{aligned} X_o &= \gamma_o\gamma_{\Phi'}\overline{MP} - k\chi_o/2 \\ X_h &= \gamma_h\gamma_{\Phi'}\overline{MP} - k\Delta\theta \sin 2\theta - k\chi_o/2. \end{aligned} \tag{17}$$

Elimination of $\overline{MP}$ in these two equations gives

$$\begin{aligned} &(X_o/\gamma_o\gamma_{\Phi'}) - (X_h/\gamma_h\gamma_{\Phi'}) \\ &\quad = (k\Delta\theta \sin 2\theta/\gamma_h\gamma_{\Phi'}) + (k\chi_o/2\gamma_h\gamma_{\Phi'}) \\ &\qquad - (k\chi_o/2\gamma_o\gamma_{\Phi'}). \end{aligned} \tag{18}$$

In this expression, $\gamma_{\Phi'}$ can be eliminated and then (18) is equivalent to equation (4.5) of Authier (1986), under the condition that the angle of asymmetry is no longer the $(\mathbf{n},\mathbf{h})$ angle as in the case of an untilted reflection but is now the $(\mathbf{n}',\mathbf{h})$ angle. Symmetric reflections will occur for $\gamma_o = |\gamma_h|$, that is to say, when $\mathbf{n}'$ and **h** are collinear, which means $\beta = \pi/2$ (Fig. 1). The $(\mathbf{h},\mathbf{k}_o^{(a)})$ and $(\mathbf{h},\mathbf{n})$ planes are then perpendicular.

## 4. Rocking curves of tilted reflections; theory and experiment

It can be shown that the reflecting power $I_h$ is a function of the dimensionless parameter $\eta$, which is related to the departure from Bragg angle $\Delta\theta = \theta - \theta_B$ by

$$\eta = (\Delta\theta - \Delta\theta_o) \sin(2\theta_B)/|C|(\chi_h\chi_{\bar{h}})^{1/2}|\gamma|^{1/2}, \tag{19}$$

where $\Delta\theta_o = -\chi_o(1-\gamma)/2 \sin(2\theta_B)$ is the deviation of the real Bragg angle from $\theta_B$ owing to the refraction. In the case of nonabsorbing crystals, $\eta$ is a real number proportional to $(\Delta\theta - \Delta\theta_o)/|\gamma|^{1/2}$ which shows that asymmetry contracts or expands the $\theta$ axis without modifying the shape of the rocking curve. This conclusion remains valid to a good extent for real absorbing crystal.

Experimentally, the measurement of the full width at half-maximum (FWHM) of the rocking curve allows one to follow the variation of the asymmetry of the reflection; the FWHM can be assimilated to the width $\omega_a$ of the total reflection domain:

$$\omega_a = 2|C|(\chi_h\chi_{\bar{h}})^{1/2}|\gamma|^{1/2}/\sin(2\theta_B) = |\gamma|^{1/2}\omega_s, \tag{20}$$

where $\omega_s$ is the FWHM for a symmetric case.

For a given position of the plane $(\mathbf{k}_o^{(a)},\mathbf{h})$, the value of the asymmetry $\gamma$ is governed by the rotation of **n** around **h**, *i.e.* the variation of the angle $\beta$. The angle $\alpha$ is related to $\beta$ by the relation

$$\tan\alpha = \cos\beta \tan\Phi, \tag{21}$$

which is illustrated in Fig. 3(*a*). The ratio of Darwin width for asymmetric ($\omega_a$) and symmetric ($\omega_s$) reflections becomes

$$\begin{aligned} \omega_a/\omega_s = &[1 - \cos\beta(\tan\Phi/\tan\theta_B)]^{1/2} \\ &\times [1 + \cos\beta(\tan\Phi/\tan\theta_B)]^{-1/2}. \end{aligned} \tag{22}$$

Let us consider the case of interest here, *i.e.* $\Phi > \theta_B$. For $\alpha$ values larger than $\theta_B$, the geometry corresponds to a transmission case. One can define two opposed critical angles $\beta = \pm\beta_c$ [$\beta_c$ = arccos (tan $\theta_B$/tan $\Phi$)] for which $\alpha = \pm\theta_B$. Grazing incidence is obtained for $\alpha = \theta_B$ and, for $\alpha = -\theta_B$, the direction of the diffracting beam is nearly parallel to the crystal surface. Fig. 3(*b*) shows that the variation of the width $\omega_a$ of the rocking curve as a function of $\beta$ depends strongly on the value of the parameter $R = \tan\Phi/\tan\theta_B$. For $R < 1$, $\omega_a$ varies smoothly with $\beta$ whereas, for $R > 1$, it varies very rapidly.

The above predictions have been experimentally checked. The sample was a (111) silicon crystal with three iron monolayers deposited on the surface. The $11\bar{1}$ reflection making an angle $\Phi = 70.52°$ to the (111) surface was used with a wavelength of 1.51 Å ($\theta_B = 13.96°$). A monolithic grooved four-reflection (+,−) monochromator for which the third reflection is asymmetric delivers a quasi-plane wave (Boulliard *et al.*, 1992). For a wavelength of 1.51 Å, the intrinsic FWHM of the rocking curve for a symmetric $11\bar{1}$ reflection is 7.25″. Taking into account the angular profile of the beam from the monochromator, one can predict $\omega_s = 7.47''$. Because of the high value of $R$ ($R = 11.41$), in order to remain in a Bragg geometry, this situation induces a small range of variation for $\beta$ ($85 \le \beta \le 95°$).

Two extreme cases of the measured rocking curves are drawn in Fig. 4 showing FWHMs of 3.20 (5)″ and 49.9 (4)″. Fig. 5 gives the experimental FWHMs as a function of $\beta$, the angle of rotation of **n** around **h**. Since the position where **h**, $\mathbf{k}_o^{(a)}$ and **n** are coplanar is not known accurately, the exact origin of the $\beta$ rotation has to be determined by a fit (line in Fig. 5) of the experimental curve with the theoretical one.

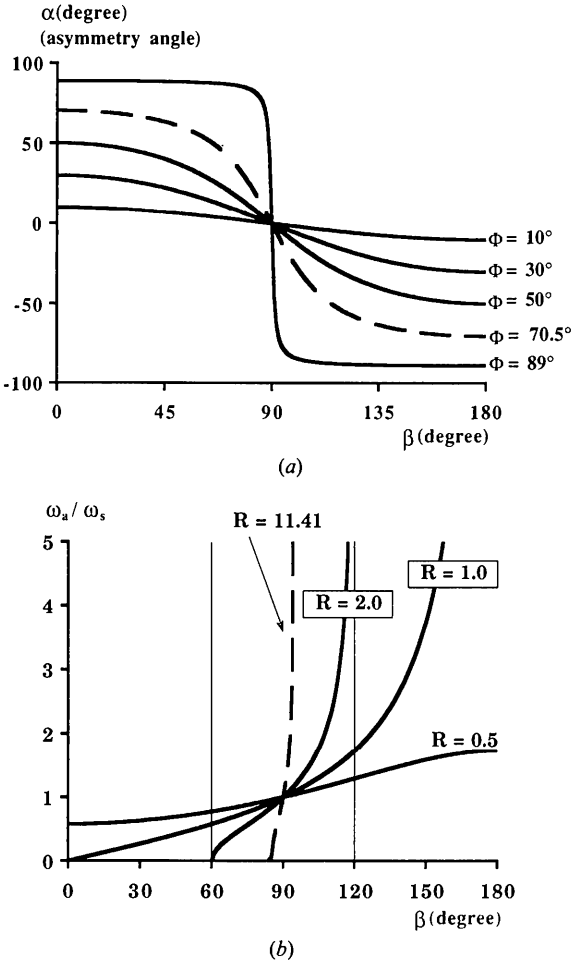


Fig. 3. (*a*) Theoretical asymmetry of an inclined reflection. Each curve corresponds to a specified angle $\Phi$. The dashed line is the case of a $11\bar{1}$ reflection on an Si(111) sample. (*b*) Theoretical ratio of the FWHMs of a tilted reflection and of a symmetric reflection as a function of the angle $\beta$ for several values of the ratio $R = \tan\Phi/\tan\theta_B$ ($\Phi$ is the angle between the reflecting planes and the surface). The dashed line is the experimental case.

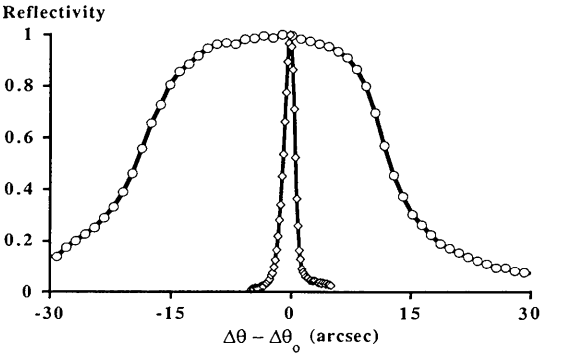


Fig. 4. Two extreme experimental $11\bar{1}$ rocking curves obtained with an Si(111) crystal.

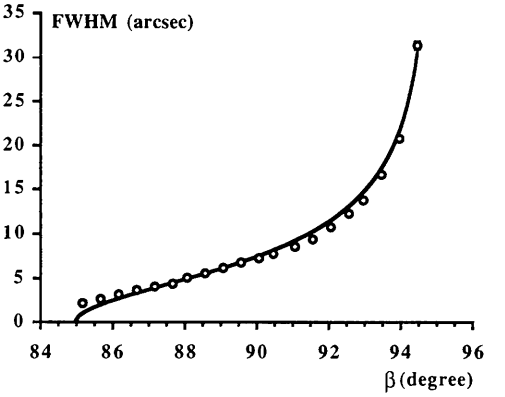


Fig. 5. Fit (full line) of the experimental measurements (circles) of FWHMs of rocking curves for a $11\bar{1}$ reflection and an Si(111) crystal as a function of $\beta$, angle of rotation of **n** around **h**.

For all $\beta$ values larger than 86°, the agreement between measurements and theory is quite good. The small FWHM (0.76″) of the beam delivered by the monochromator has not been taken into account to calculate the curve. This explains the small difference between the experimental and theoretical values for $\beta < 86°$. This experiment shows that it is possible to obtain controlled asymmetric reflections by using tilted reflections.

### 5. Tilted reflections for an XSW experiment

As shown in § 4, for large values of $R = \tan \Phi/\tan \theta_B$, a small variation of $\beta$ induces large modifications of the shape of the rocking curve. How is the fluorescence yield then modified?

Combining (5) and (9), one gets for the fluorescence yield

$$Y(\eta) \simeq 1 + I_h(\eta)/|\gamma| + 2C[I_h(\eta)/|\gamma|]^{1/2} F_h \times \cos[\psi(\eta) + 2\pi P_h]. \quad (23)$$

As shown previously, the effect of asymmetry is to contract or expand the rocking curve along the $\theta$ axis. The same holds for $\psi(\theta)$. In contrast, (23) shows that asymmetry modifies the fluorescence in a more complicated way and the following results show the importance of taking it into account correctly.

Three experiments have been performed on the sample described in § 4 using the same $11\bar{1}$ reflection for three slightly different values of $\beta$, $\beta_o$, $\beta_o + 0.6°$ and $\beta_o - 0.5°$, with $\beta_o$ near 90°, which is the symmetric case value. The results are shown in Fig. 6. The rocking curves are very similar and, if each experiment had been performed separately, each of them would have probably been considered as a symmetric case. In contrast, fluorescence Fe $K\alpha$ curves are quite different and would have led, for a symmetric geometry, to different values of $F_h$ and $P_h$ (Table 1). These three experimental results have been fitted using asymmetry as a parameter. Results are presented in Table 1 and show that the values of $F_h$ and $P_h$ thus determined are now the same. If the asymmetry is not taken into account, results for $P_h$ could vary from 0.11 to 0.19, leading to large errors in the atomic positions. The interplanar $(11\bar{1})$ distance being 3.13 Å, the atomic position thus determined would have varied from 0.34 to 0.59 Å. This example shows the crucial importance of a precise fit of the rocking curve taking into account the exact geometry of the diffraction.

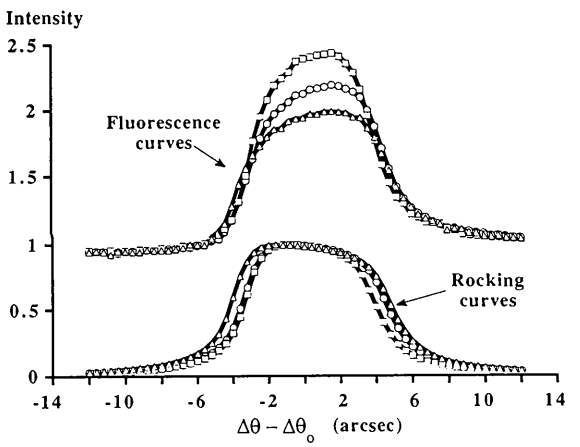


Fig. 6. $(11\bar{1})$ rocking curves and fluorescence Fe $K\alpha$ yields for an Si(111) crystal with three iron monolayers deposited and three different values of the asymmetry angle $\alpha$. Squares: $\alpha = +1.75°$. Circles: $\alpha = +0.12°$. Triangles: $\alpha = -1.34°$.

Table 1. *Modulus and phase of the XSW structure factor for the three experiments made on a* (111) *silicon sample with three monolayers of iron using the* $11\bar{1}$ *reflection*

The third and fourth columns are the coherent function $F_h$ and the coherent position $P_h$ when the asymmetry is taken into account; the last two columns are their values obtained assuming a symmetric case.

| | $\beta$ (°) | Fitted asymmetry ($\alpha$) (°) | $(F_h)_\alpha$ | $(P_h)_\alpha$ | $(F_h)_{\alpha=0°}$ | $(P_h)_{\alpha=0°}$ |
|---|---|---|---|---|---|---|
| Experiment 1 | $\beta_o+0.6$ | +1.75 | 0.22 (1) | 0.16 (1) | 0.34 (1) | 0.19 (1) |
| Experiment 2 | $\beta_o$ | +0.12 | 0.22 (1) | 0.16 (1) | 0.22 (1) | 0.16 (1) |
| Experiment 3 | $\beta_o-0.5$ | −1.34 | 0.22 (1) | 0.16 (1) | 0.18 (1) | 0.11 (1) |

### 6. Concluding remarks

X-ray dynamical theory has been applied to the cases where reflecting planes are inclined with respect to the surface and tilted geometries (*i.e.* when the normal to the crystal surface, the incident wave vector and the diffraction vector are not coplanar) are used.

Tilted geometries are often necessary to fully determine by the XSW technique the position of adatoms with respect to the crystal lattice, and it has been shown that the exact value of the asymmetry, which can vary very rapidly with small changes of the orientation of the crystal for very inclined diffracting planes, must be determined carefully to obtain reliable results. This is especially important for very inclined diffracting planes; nevertheless, our results show that, whatever the geometry is, an error of the order of 1° in the asymmetry angle $\alpha$ can induce noticeable errors in the atomic position.

Most generally, tilted geometries offer the possibility of obtaining Bragg geometry for any reflecting plane in the crystal with any value of the asymmetry (including the symmetric case), which is very interesting for several X-ray optics applications. For instance: (i) there is the possibility of varying freely

the asymmetry and then the width of the rocking curve by a simple rotation of the sample; (ii) the use of very inclined reflecting planes in a tilted and symmetric geometry enables a decrease in the thermal load on monochromators, since the trace of the incident beam on the surface of the crystal is then much larger than in the case of symmetric reflections on the surface (Macrander *et al.*, 1992).

The experiments were performed on beam line D15B of the DCI storage ring at LURE, Orsay, France. We thank very much Professor J. Derrien of the CRMC2, Marseille, France, for the preparation of the sample. This work was financially supported by the French Ministry of Research and the EEC (Esprit BRA no. 3026).

**References**

AUTHIER, A. (1986). *Acta Cryst.* A**42**, 414–426.
BATTERMAN, B. W. (1964). *Phys. Rev. A*, **133**, 759–764.
BATTERMAN, B. W. (1969). *Phys. Rev. Lett.* **22**, 703–705.
BEDZYK, M. J., GIBSON, W. M. & GOLOVCHENKO, J. A. (1982). *J. Vac. Sci. Technol.* **20**, 634–637.
BEDZYK, M. J. & MATERLICK, G. (1985). *Surf. Sci.* **152/153**, 10–16.
BOULLIARD, J. C., CAPELLE, B., FERRET, D., LIFCHITZ, A., MALGRANGE, C., PÉTROFF, J. F., TACCOEN, A. & ZHENG, Y. L. (1992). *J. Phys.* I (France), **2**, 1215–1232.
MACRANDER, A. T., LEE, W. K., SMITH, R. K., MILLS, D. M., ROGERS, C. S. & KHOUNSARY, A. M. (1992). *Nucl. Instrum. Methods Phys. Res.* A**319**, 188–196.
SAITOH, Y., HASHIZUME, H. & TSUTSUI, K. (1988). *Jpn. J. Appl. Phys.* **27**, 1386–1396.
VLIEG, E., FONTES, E. & PATEL, J. R. (1991). *Phys. Rev. B*, **43**, 7185–7193.
ZEGENHAGEN, J. (1993). *Surf. Sci. Rep.* **18**, 199–271.

*Acta Cryst.* (1994). A**50**, 503–510

# The *Ab Initio* Crystal Structure Solution of Proteins by Direct Methods. I. Feasibility

BY CARMELO GIACOVAZZO AND DRITAN SILIQI*

*Dipartimento Geomineralogico, Università di Bari, Campus Universitario, Via Orabona* 4, 70125 *Bari, Italy*

AND ADAM RALPH†

*Istituto di Strutturistica Chimica 'G. Giacomello', CNR, Area della Ricerca, CP* 10, 00016 *Monterotondo Stazione, Roma, Italy*

(*Received* 8 *October* 1993; *accepted* 4 *January* 1994)

## Abstract

Traditional direct methods based on the tangent formula and/or on Sayre's equation cannot solve *ab initio* the large majority of protein crystal structures [Giacovazzo, Guagliardi, Ravelli & Siliqi (1994). *Z. Kristallogr.* **209**, 136–142]. Indeed, the amount of information available leads to a signal-to-noise ratio close to unity; consequently, the correct solution, even if attained, cannot be recognized among the trial solutions. Attention is here focused onto the case in which diffraction data of one isomorphous derivative are additionally available. It is shown that in such a case direct *ab initio* solution of protein structures is feasible. Tests based on calculated diffraction data suggest the procedure to follow for a possible success.

## Notation

| | |
|---|---|
| $F_p = \|F_p\| \exp(i\varphi)$ | Structure factor of the protein |
| $F_d = \|F_d\| \exp(i\psi)$ | Structure factor of the isomorphous derivative |
| $F_H = F_d - F_p$ | Structure factor of the heavy-atom structure (added to the native protein) |
| $\Phi = \varphi_{\mathbf{h}} - \varphi_{\mathbf{k}} - \varphi_{\mathbf{h}-\mathbf{k}}$ | |
| $E_p = R \exp(i\varphi)$ | Normalized structure factor for the protein |
| $E_d = S \exp(i\psi)$ | Normalized structure factor for the isomorphous derivative |
| $N$ | Number of non-H atoms in the primitive cell |
| $\sigma_i = \sum_{j=1}^{N} Z_j^i$ | ($Z_j$ is the atomic number of the $j$th atom) |
| $N_{\rm eq} = \sigma_2^3/\sigma_3^2$ | Statistically equivalent number of atoms in the primitive unit cell |
| $[\sigma_2^3/\sigma_3^2]_p$ | Value of $N_{\rm eq}$ for the native protein |
| $[\sigma_2^3/\sigma_3^2]_H$ | Value of $N_{\rm eq}$ relative to the heavy-atom structure |

* Present address: Laboratory of X-ray Diffraction, Department of Inorganic Chemistry, Faculty of Natural Sciences, Tirana University, Tirana, Albania.

† Present address: Department of Chemistry, University of Manchester, Oxford Road, Manchester M13 9PL, England.